Supporting Information

Enhanced Intrinsic White-Light Emission Upon Near-UV Excitation by Crystal Engineering of Cationic Lead Bromide Layered Materials

Huimin Yang,[a]‡ Jinlin Yin,[a]‡ Xiaoxiang Xu*[a,b] and Honghan Fei *[a]

[a] School of Chemical Science and Enginnering, Shanghai Key Laboratory of Chemical Assessment and Sustainability, Tongji University, Shanghai 200092, P. R. China

[a] Clinical and Central Lab, Putuo People's Hospital, Tongji University, 1291 Jiangning Road, Shanghai, 200060, P. R. China

Experimental

Synthesis of $[Pb_4Br_6][O_2C(CH_2)_6CO_2]$ (TJU-8). A mixture of $PbBr_2$ (99.0%, Aladdin) (0.36 g, 1 mmol) and suberic acid (98%, Adamas) (0.35 g, 2.1 mmol) were added into the 15 mL Teflon-lined autoclave and heated at 150 ^oC for 72 h. After cooling down to room temperature, the crystals were isolated by centrifugation, and washed by deionized water and ethanol for three times and dried at 60 ^oC under atmospheric condition. Yield 59 mg (16 % based on total Pb content). The μm-sized microscopic powders of TJU-8 were prepared via grinding the bulk crystals.

Synthesis of $[Pb_2Br_2][O_2C(CH_2)_6CO_2]$ (TJU-9). Suberic acid (0.35 g, 2.1 mmol) was dissolved in sodium hydroxide solution (168 mg, 4.2 mmol) and excess ethanol was added in the solution to crystallize the disodium suberate. A mixture of $PbBr_2$ (99.0%, Aladdin) (0.36 g, 1 mmol), disodium suberic acid (0.4 g, 1.8 mmol) and 200 μL perchloric acid ($HClO_4$, 2.4 mmol) were added into the 15 mL Teflon-lined autoclave and heated at 175 ^oC for 72 h. After cooling down to room temperature, the products were washed by deionized water and ethanol for three times and dried at 60 ^oC. Yield 240 mg (64 % based on total Pb content). The μm-sized microscopic powders of TJU-9 were prepared via grinding the bulk crystals.

Single Crystal X-ray Diffraction (SCXRD). Single crystal data were recorded using a Bruker APEX II CCD area detector X-ray diffractometer using graphite monochromated Mo-Kα (λ = 0.71073 Å). The structures were solved by direct methods and expanded routinely. The models were refined by full-matrix

least-squares analysis of F^2 against all reflections. All non-hydrogen atoms were refined with anisotropic thermal displacement parameters. Programs used: APEX-II v2.1.4; SHELXTL v6.14; Diamond v3.2.

Powder X-ray Diffraction (PXRD). PXRD data were collected at ambient temperature on a Bruker D8 Advance diffractometer at 40 kV, 40 mA for Cu Kα (λ=1.5418 Å), with a scan speed of 0.2 sec/step, a step size of 0.02° in 2θ, and a 2θ range of ~5 to 45 ° (5 ° for TJU-8 and 4.5 ° for TJU-9). Simulated powder patterns were calculated by Mercury software using the crystallographic information file from the single-crystal X-ray experiment.

Fourier-transform infrared spectrum (FT-IR). FT-IR spectra were performed on a BRUKER ALPHA spectrophotometer in the region of 4000~400 cm-1 with a resolution of 2 cm^{-1}.

Thermogravimetry analysis (TGA). Thermogravimetric analyses were performed in N_2 stream (60 mL/min) on a NETZSCH STA 409 PC/PG differential thermal analyser running from room temperature to 800 °C with a heating rate of 10 °C/min.

Chemical and thermal stability studies. Appropriate amounts of TJU-8 and TJU-9 were incubated in boiling water, a HCl solution, and a NaOH solution, respectively, for 24 h. PXRD analysis was performed after isolating the crystals by centrifugation. To test the thermal stability of materials, TJU-8 and TJU-9 were heated in air at

different temperature (250°C for TJU-8 and 200°C for TJU-9) and then tested by PXRD.

Optical Absorption Spectroscopy. Optical absorption spectroscopy measurements were performed on a Shimadzu UV-2600 UV-VIS spectrometer equipped with an integrating sphere, operating at room temperature in the 200-1000 nm region.

Steady state photoluminescence. Steady-state photoluminescence spectra were obtained at room temperature on an Edinburgh Instruments FLS980 spectrophotometer.

Photoluminescence quantum efficiencies (PLQEs). Absolute PLQE measurements were performed on FLS 920 spectrophotometer with an integrating sphere ($BaSO_4$ coating) in single photon counting mode. The focal length of the monochromator was 300 mm. Samples were excited at 375 nm (TJU-8) and 376 nm (TJU9) by a 450W Xenon lamp with 3 mm excitation slits width and detected by a Hamamatsu R928p photomultiplier tube. The emission was obtained using 0.2 nm scan step, 0.2 s scan dwell time, and 0.1 mm emission slit width. The PLQEs were calculated by the equation: $\varphi = k_f/k_a$, in which k_f means the number of emitted photons and k_a means the number of absorbed photons.

Time-resolved photoluminescence. Time-resolved emission data was collected using the FLS980 spectrophotometer at room temperature. The average lifetime was simulated by bi-exponential decays according to the equation:

$$\tau_{avg} = \frac{\Sigma\ a_i\tau_i^2}{\Sigma\ a_i\tau_i} \quad i = 1, 2$$

In which a_i represents the amplitude of each component and τ_i represents the decay time.

Temperature-dependent photoluminescence. Temperature-dependent emission data was collected from the FLS980 spectrophotometer at a series of temperature from 77 K to 330 K.

Photostability studies. A 4 W, 365 nm UV lamp was used as the continuous irradiation source to test the photostability of TJU-8 and TJU-9. After 30 days irradiation, steady-state photoemission measurements were performed for samples that are irradiated in air (~60% relative humidity, room temperature).

Raman measurements. The solid-state Raman spectra were performed on a CRIAC 20/30PV Technologoes microspectrophotometer with an excitation wavelength of 785 nm. Crystals were placed on slides, and data was collected after optimization of microspectrophotometer.

Computational Methods. Band gap calculations were carried out using density functional theory (DFT) implemented in the Vienna Ab initio Simulation Package (VASP)[S1]. The Perdew, Burke and Ernzerhof (PBE) exchange-correlation functional within the generalized gradient approxiamtion (GGA)[S2] and the projector augmented-wave pseudopotential were used[S3]. Monoclinic unit cells (a = 14.67 Å, b =

8.49 Å, c = 8.35 Å, $\alpha = \gamma = 90^{o}$ and $\beta = 90.75^{o}$) and (a = 34.88 Å, b = 13.23 Å, c = 8.99 Å, $\alpha = \gamma = 90^{o}$ and $\beta = 98.08^{o}$) was built for TJU-8 and TJU-9 simulations, respectively. All geometry structures were fully relaxed until the forces on each atom are less than 0.01 eV/ Å. Static calculations were done with 3×5×5 and 1×3×5 Monkhorst-Pack *k*-point grid for TJU-8 and TJU-9, respectively[S4]. Excited-state calculations were performed by using the CP2K package. Perdew-Burke-Ernzerhof (PBE) functional with Grimme D3 correction was used to describe the system. Unrestricted Kohn-Sham DFT has been used as the electronic structure method in the framework of the Gaussian and plane waves method. The Goedecker-Teter-Hutter (GTH) pseudopotentials, DZVP-MOLOPT-SR-GTH basis sets were utilized to describe the molecules. A plane-wave energy cut-off of 500 Ry has been employed. The lattice parameters were fixed at the experimentally measured values while the atomic positions were optimized. Following Franck-Condon principle, the optical excitation and emission energies were obtained by calculating the total energy differences between the excited and the ground states using optimized ground-state and excited-state structures, respectively.

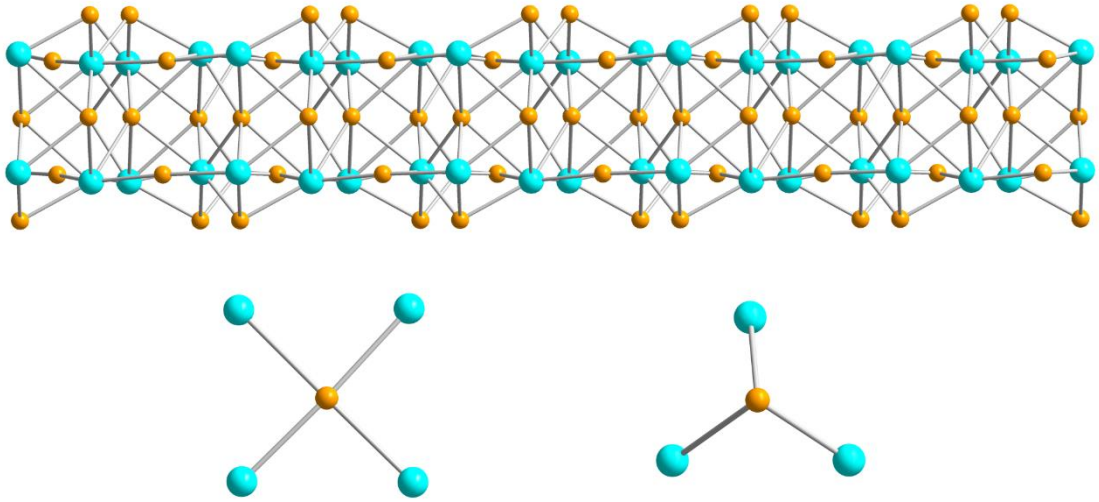

Figure S1. A single $[Pb_4Br_6]^{2+}$ layer of TJU-8 and the coordination environment of two crystallographic independent Br atoms .

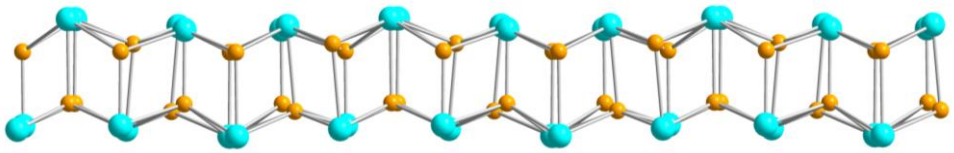

Figure S2. A single $[Pb_2Br_2]^{2+}$ layer of TJU-9

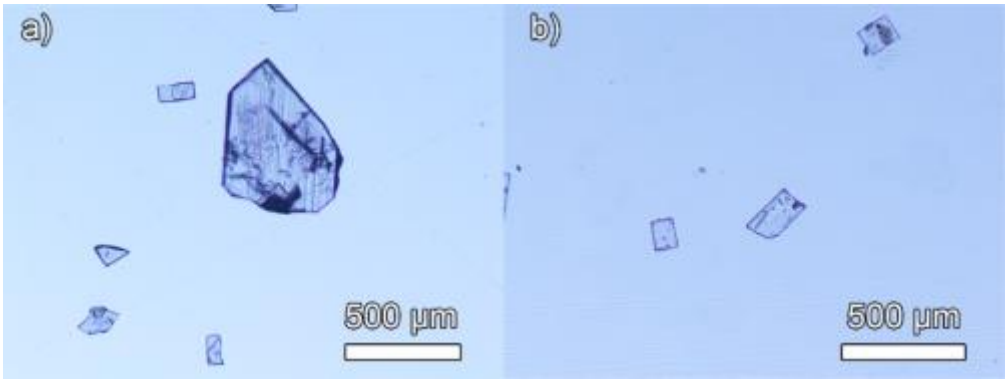

Figure S3. Optical microscope image of TJU-8 (a) and TJU-9 (b)

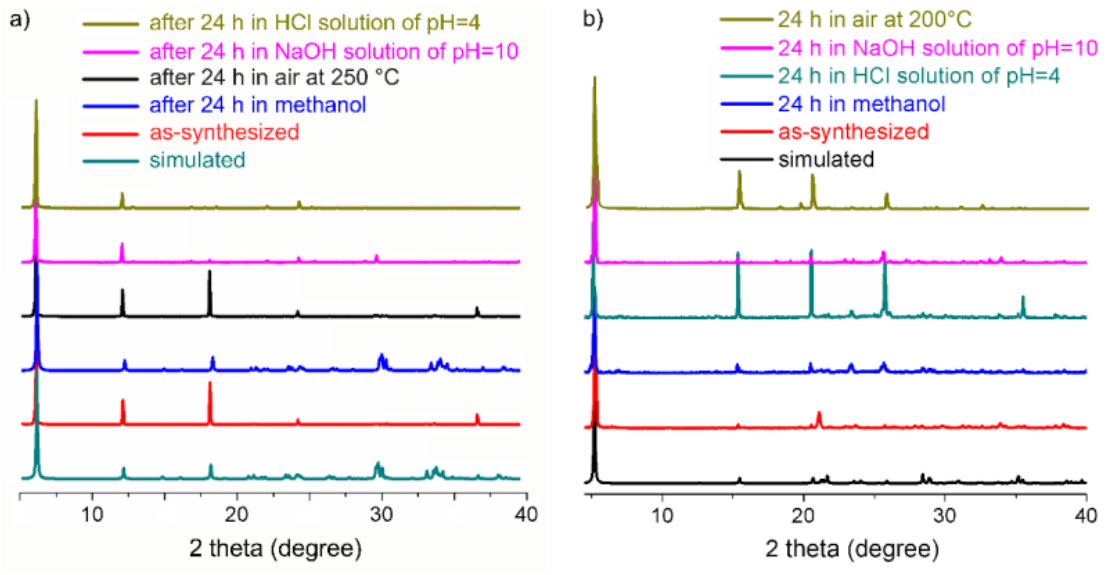

Figure S4. XRD pattern of TJU-8 (a) and TJU-9 (b) before and after thermal and chemical treatment.

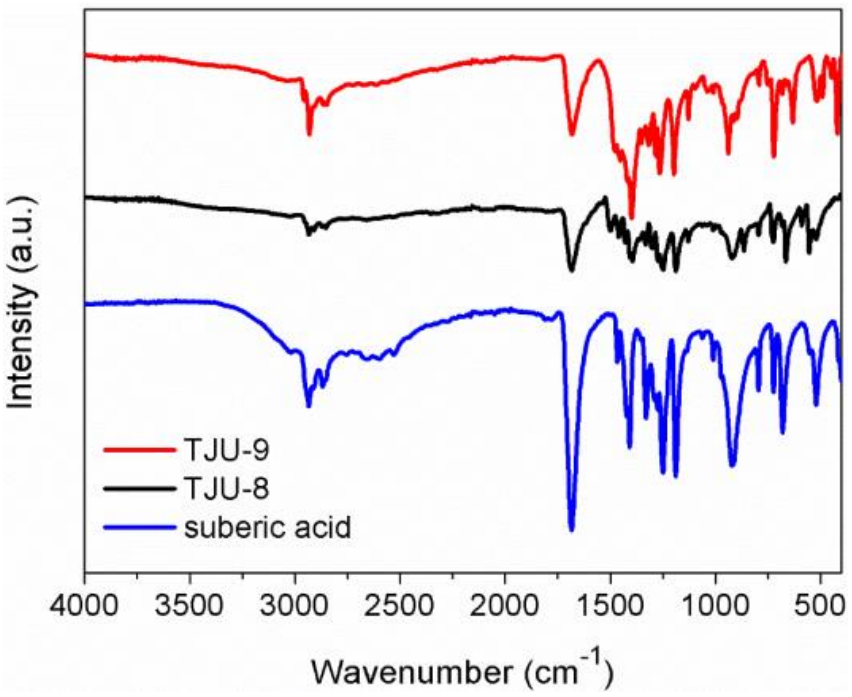

Figure S5. FT-IR spectra of TJU-8 and TJU-9.

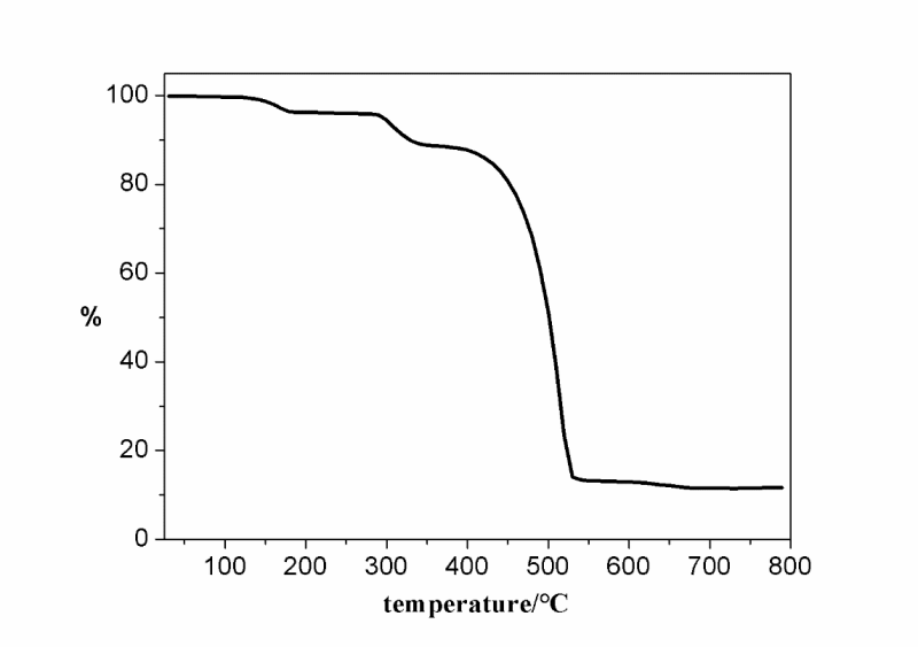

Figure S6. Thermogravimetric analysis curve of TJU-8 in N_2 flow.

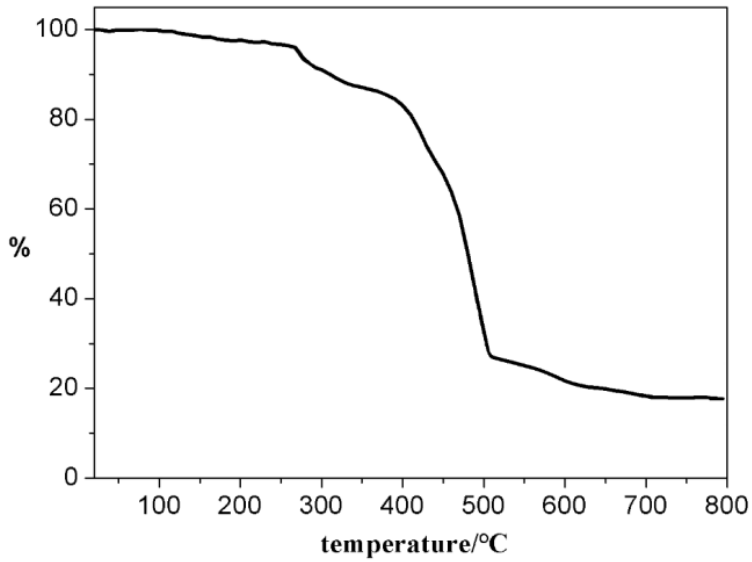

Figure S7. Thermogravimetric analysis curve of TJU-9 in N_2 flow.

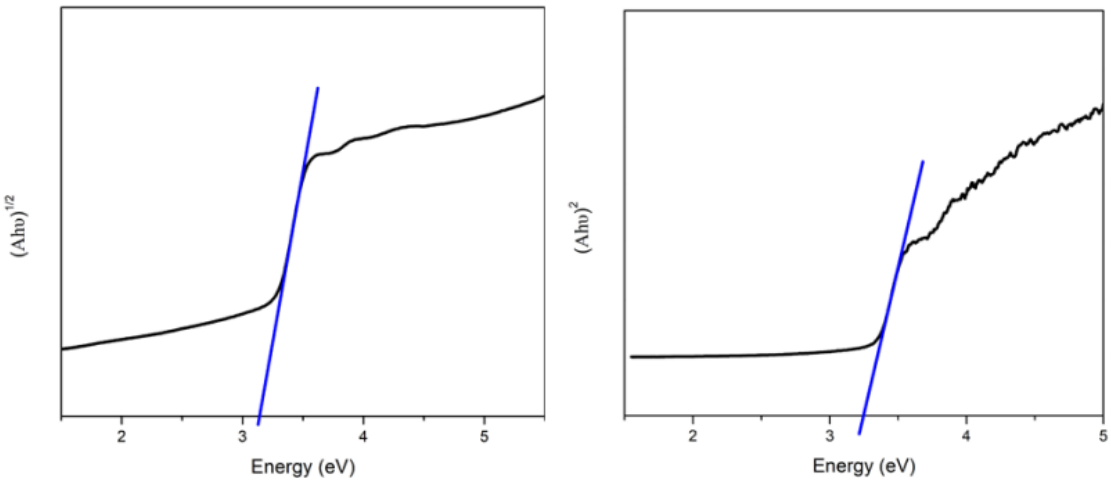

Figure S8. The tauc plot, $(A*h\upsilon)^n$ (n = 2 or 1/2) as a function of photon energy (hυ). The bandgap of TJU-8 and TJU-9 were estimated as 3.14eV and 3.25 eV by extrapolation of the linear region, respectively.

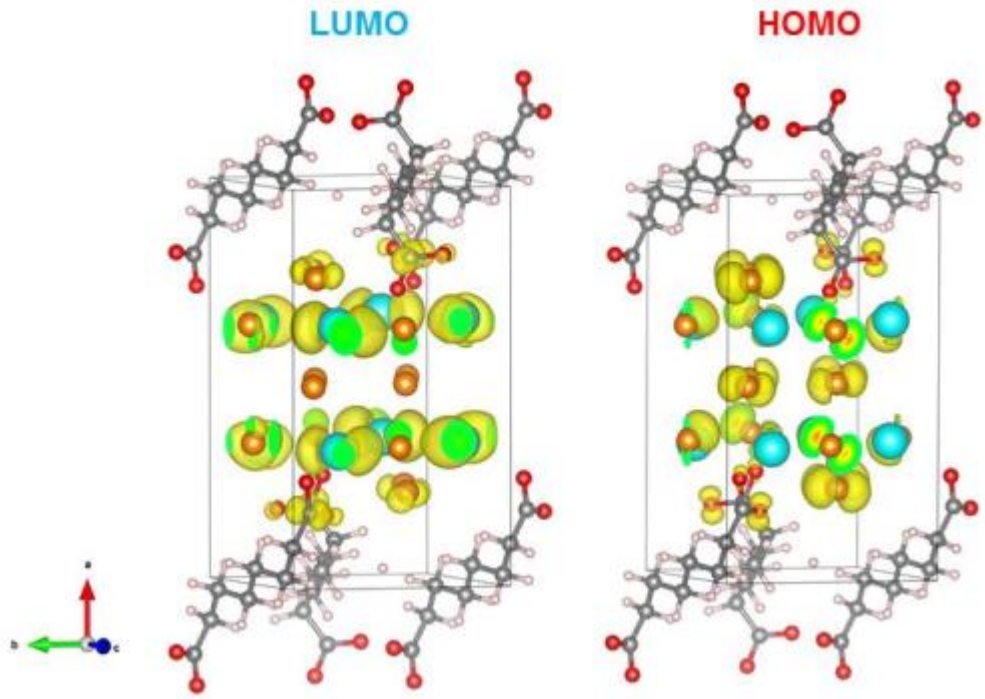

Figure S9. Density contour maps of lowest unoccupied molecular orbitals (LUMO) and highest occupied molecular orbitals (HOMO) for TJU-8, unit cell is marked by dark line.

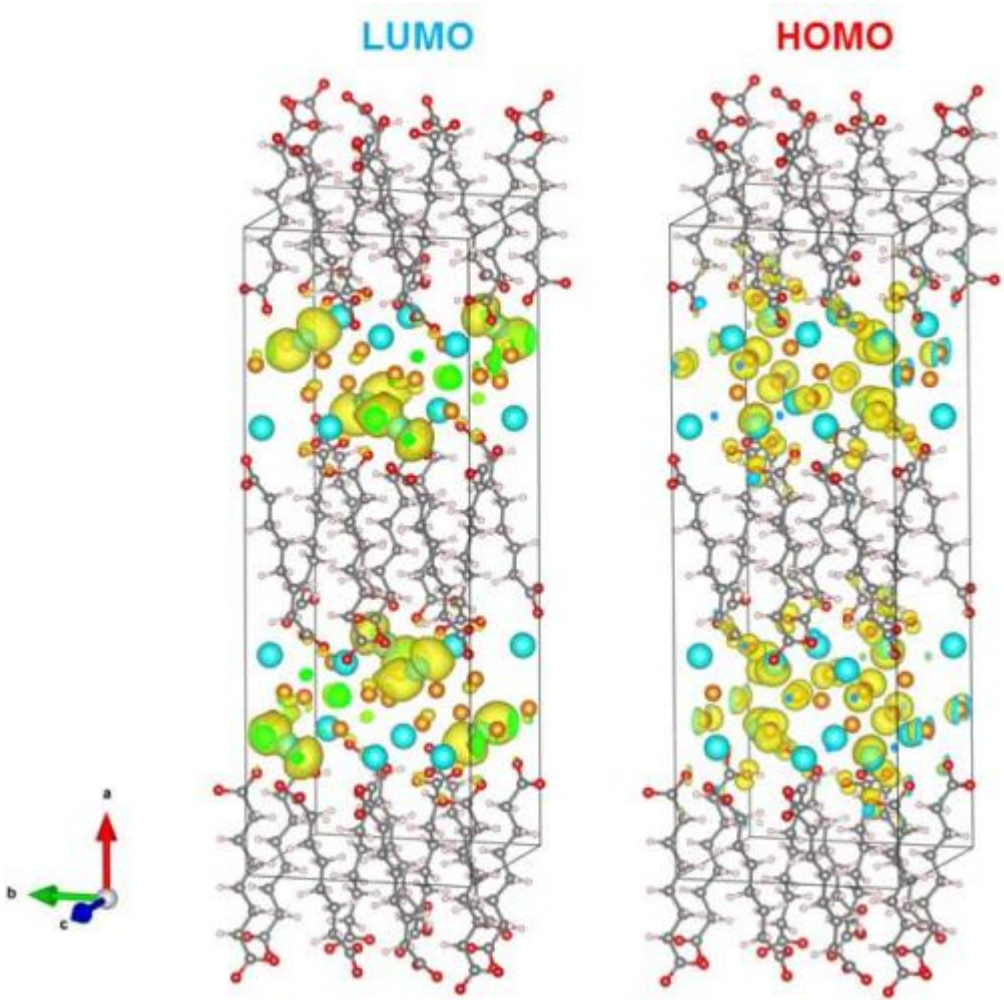

Figure S10. Density contour maps of lowest unoccupied molecular orbitals (LUMO) and highest occupied molecular orbitals (HOMO) for TJU-8, unit cell is marked by dark line.

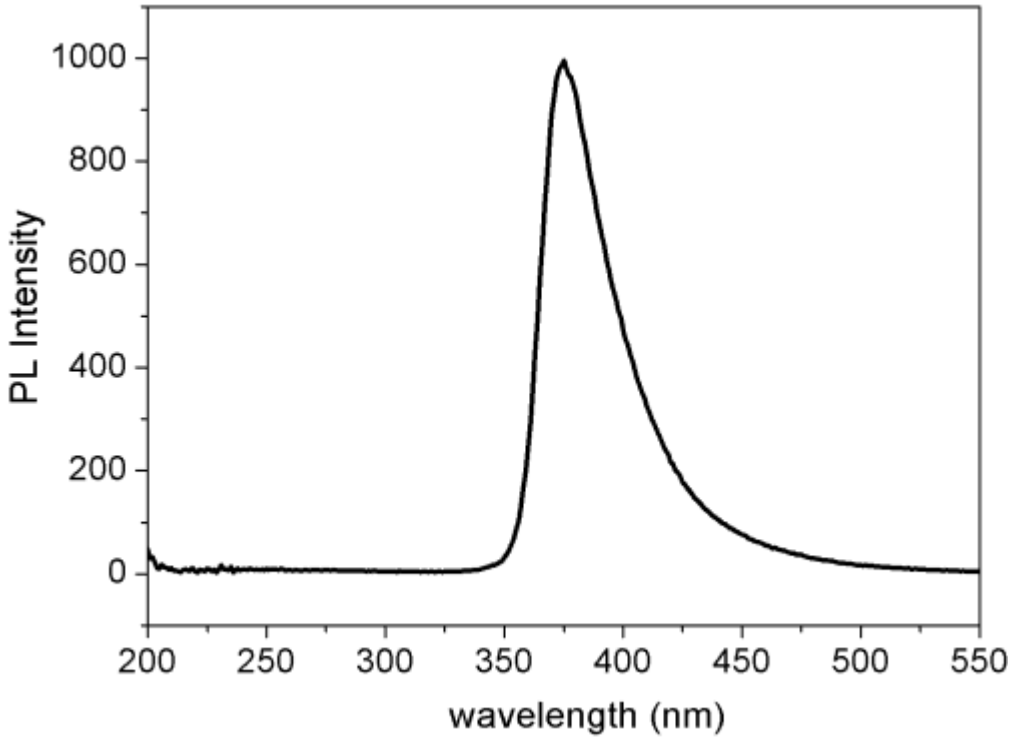

Figure S11. Excitation spectrum of TJU-8.

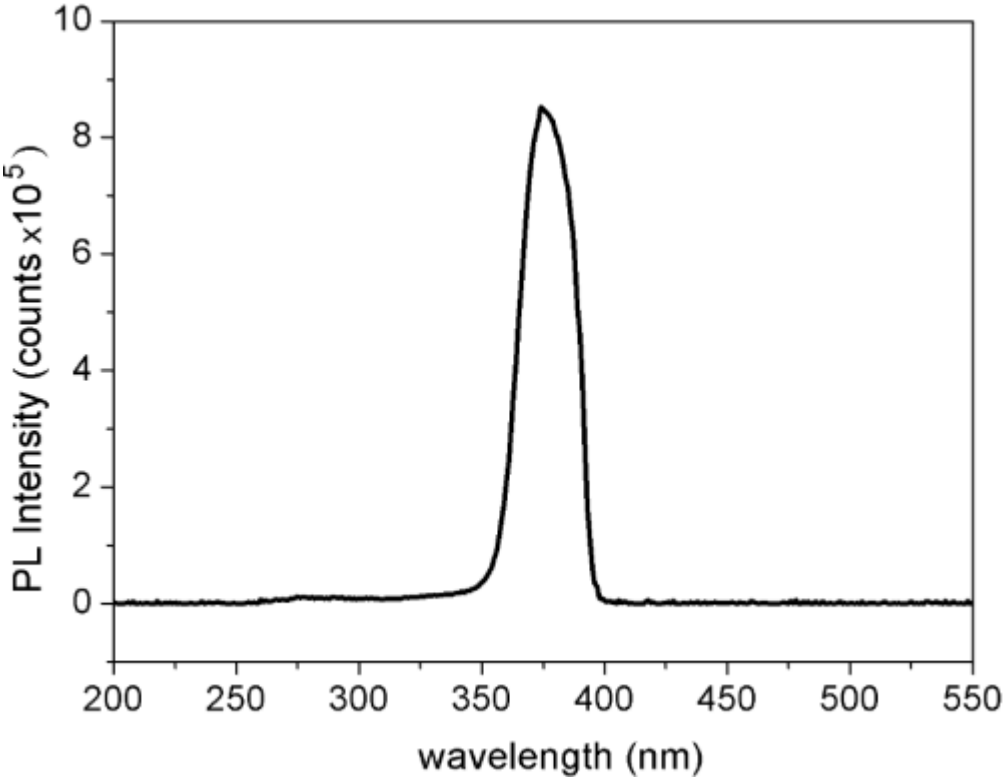

Figure S12. Excitation spectrum of TJU-9.

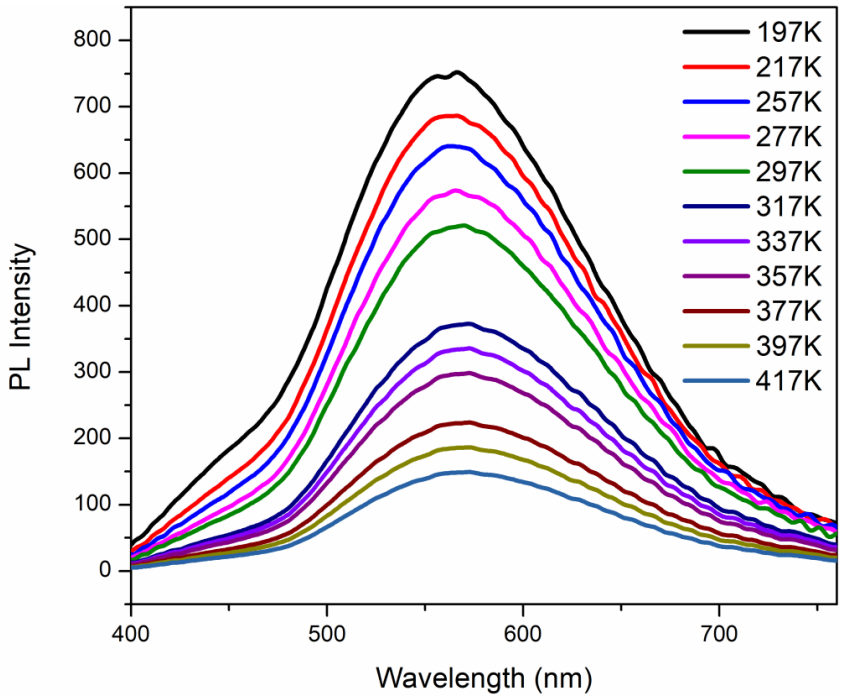

Figure S13. Temperature-depended emission spectra of TJU-9.

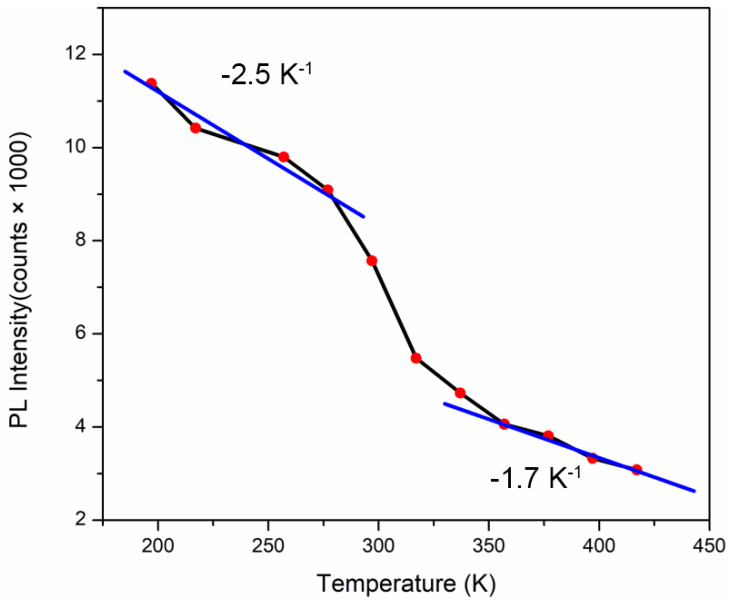

Figure S14. Temperature-dependent decay of the emission intensity in TJU-8.

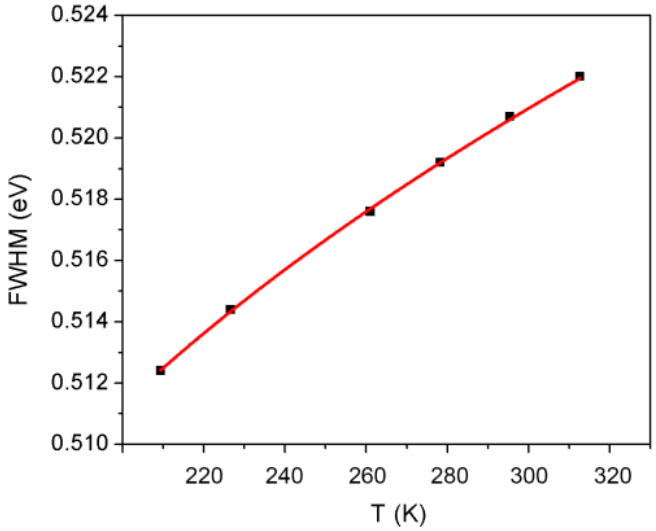

Figure S15. Temperature-dependent FWHM of the emission band in TJU-8 (black symbols) and the best fit to eq. 3 in the manuscript (red line).

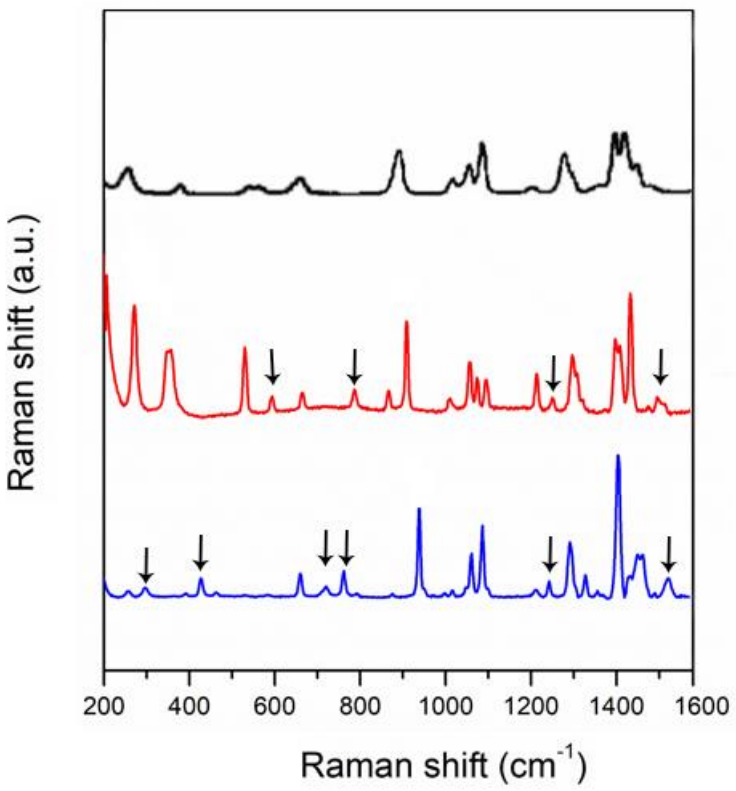

Figure S16. Raman spectra of TJU-9 (blue), TJU-8 (red), and suberic acid (black). The new active modes of suberate upon TJU-8 and TJU-9 formation are indicated by the black arrows.

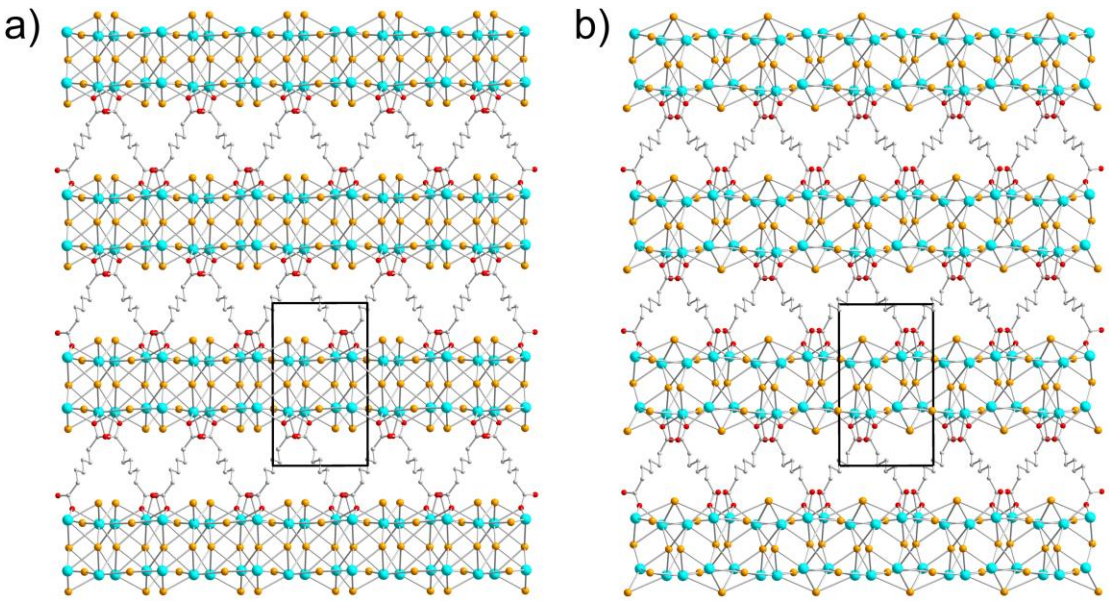

Figure S17. Crystallographic view of ground-state TJU-8 (a) and excited-state TJU-8 (b) along the *c*-projection.

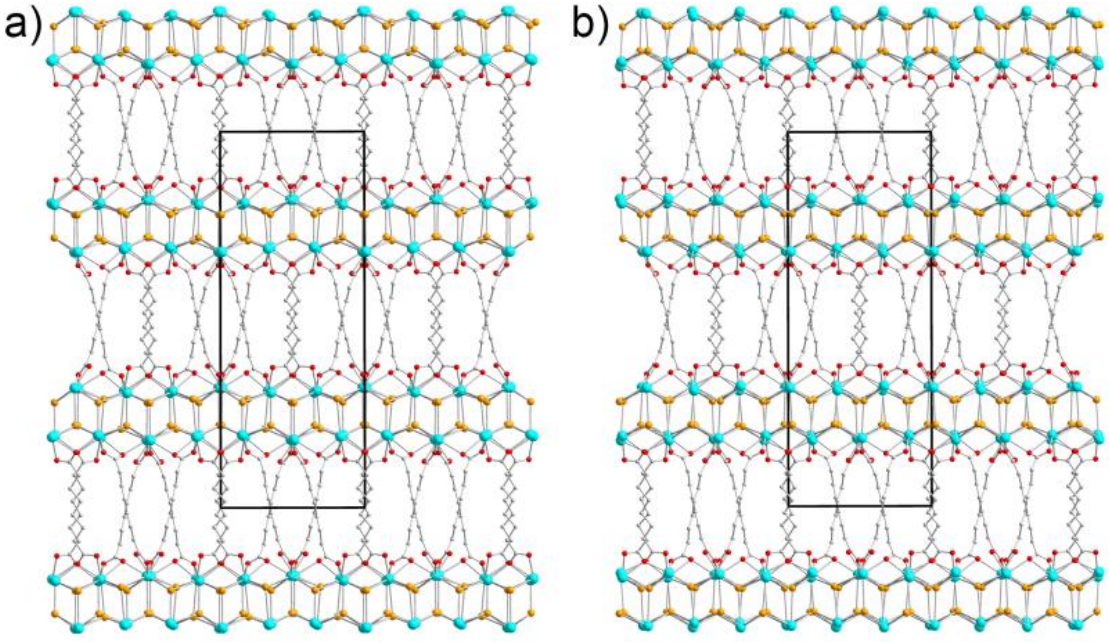

Figure S18. Crystallographic view of ground-state TJU-9 (a) and excited-state TJU-9 (b) along the *c*-projection.

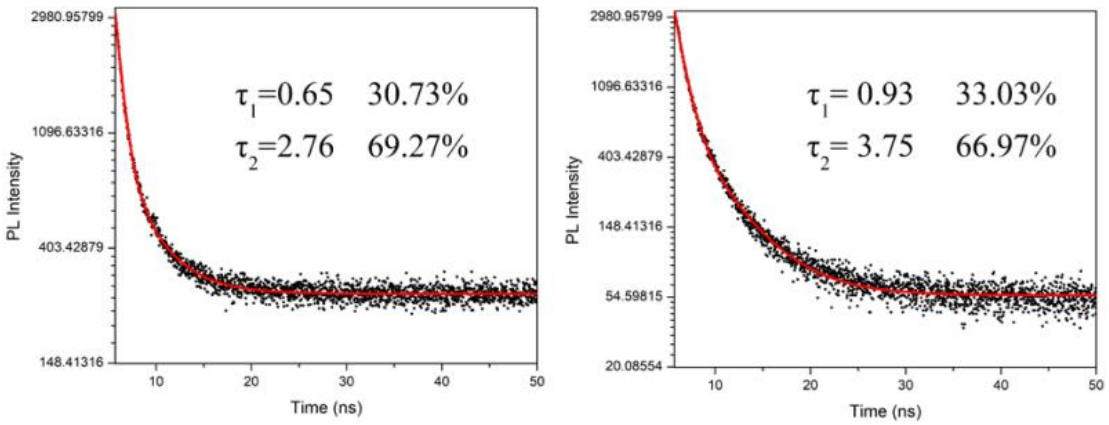

Figure S19. The PL decay of crystals with the fit to data (red line) of TJU-8 (left) and TJU-9 (right). The radiative decay rates were calculated to be approximately $2.81\times10^7\ s^{-1}$ and $2.90\times10^7\ s^{-1}$, and the non-radiative decay rates of approximately $31.39\times10^7\ s^{-1}$ and $32.4\times10^7\ s^{-1}$ for TJU-8 and TJU-9, respectively.

Table S1. Crystal data and structure refinement for TJU-8 and TJU-9.

Compound	λ_{Pb1}	λ_{Pb2}	λ_{Pb3}	λ_{Pb4}	λ_{avg}
α-(DMEN)$PbBr_4$[S5]	30.8	4.0			17.4
(DMAPA) $PbBr_4$[S5]	1.1				1.1
(DMABA) $PbBr_4$[S5]	3.0	7.4	1.3	5.4	4.3
(API) $PbBr_4$[S6]	26.0				26.0
(AETU) $PbBr_4$[S7]	9.7				9.7
(N-MEDA) $PbBr_4$[S8]	8.2				8.2
TJU-8	**32.4**				**32.4**
TJU-9	**26.9**	**25.0**	**3.15**		**18.4**

Table S2. A Comparison between DFT Calculated and Experimental Photophysical Properties.

Materials	DFT Calculations		Experimental Results	
	E_{ex} (eV)	E_{em} (eV)	E_{ex} (eV)	E_{em} (eV)
TJU-8	3.56	2.28	3.31	2.23
TJU-9	3.89	1.80	3.30	2.19

Table S3. Crystal data and structure refinement for TJU-8 and TJU-9.

	TJU-8	TJU-9
Empirical formula	$C_4H_6O_2Br_3Pb_2$	$C_{12}H_{20}O_7Br_3Pb_3$
Formula weight/ g mol^{-1}	740.2	1132.54
Temperature/ K	273(2)	300(2)
Crystal system	monoclinic	monoclinic
Space group	$P2_1/c$	C2/c
Unit cell dimensions	a = 14.574(5) Å	a = 34.884(5) Å
	b = 8.493(3) Å	b = 13.226(2) Å
	c = 8.347(3) Å	c = 8.9982(15) Å
	β = 90.753(14) deg	β = 98.082(6) deg
Volume/ $Å^3$	1033.08(60)	4110.4(12)
Z	4	8
Density/ g cm^{-3}	4.759	3.660
Absorption coefficient (μ)/ mm^{-1}	44.109	30.377
F(000)	1260.0	3952.0
2θ range for data collection/ deg	5.552 to 50.678	6.16 to 53.464
	$-15 \le h \le 17$,	$-44 \le h \le 44$
Index ranges	$-10 \le k \le 10$	$-16 \le k \le 16$
	$-10 \le l \le 10$	$-11 \le l \le 10$
Reflections collected	6916	30312
Independent reflections	1869[R(int) = 0.0701]	4364[R(int) = 0.0828]
Data / restraints / parameters	1869/12/101	4364/0/226
Goodness-of-fit on F^2	1.075	1.192
Final R indices [I>2sigma(I)]	R1 = 0.0885	R1 = 0.1142
	wR2 = 0.2395	wR2 = 0.3189
R indices (all data)	R1 = 0.1110	R1 = 0.1317
	wR2 = 0.2628	wR2 = 0.3285

$R_1=\Sigma(||F_o|-|F_c||) / \Sigma|F_o|$; $wR_2=\{\Sigma[w(F_o^2-F_c^2)^2]/\Sigma[w(F_o^2)]^2\}^{1/2}$

References

S1 Kresse, G., Furthmuller, J. *Phys. Rev. B* **1996**, *54*, 11169-11186.

S2 Perdew, J. P., Burke, K., Ernzerhof, M. *Phys. Rev. Lett.* **1996**, *77*, 3865-3868.

S3 Kresse, G., Joubert, D. *Phys. Rev. B* **1999**, *59*, 1758-1775.

S4 Monkhorst, H. J., Pack, J. D. *Phys. Rev. B* **1976**, *13*, 5188-5192.

S5 Mao, L., Wu, Y., Stoumpos, C. C., Wasielewski, M. R., Kanatzidis, M. G. *J. Am. Chem. Soc.* **2017**, *139*, 5210-5215.

S6 Yin, J., Li, G., Cortecchia, D., Soci, C., Bredas, J.-L. *ACS Energy Lett.* **2017**, *2*, 417-423.

S7 Li, Y., Zheng, G., Lin, J. *Eur. J. Inorg. Chem.* **2008**, *2008*, 1689-1692.

S8 Dohner, E. R., Hoke, E. T., Karunadasa, H. I. *J. Am. Chem. Soc.* **2014**, *136*, 1718-1721.